Amorphous Orientation and Its Relationship to Processing Stages of Blended Polypropylene/ Polyethylene Fibers

Amy M. Trottier,[1,2] J. W. Zwanziger,[1,2] N. Sanjeeva Murthy[3*]

[1]*Department of Chemistry, Dalhousie University, Halifax, Nova Scotia, Canada B3H 4J3*
[2]*Institute for Research in Materials, Dalhousie University, Halifax, Nova Scotia, Canada B3H 4J3*
[3]*Physics Department, University of Vermont, Burlington, Vermont 05405*

Received 4 September 2007; accepted 20 December 2007
DOI 10.1002/app.28016
Published online 19 March 2008 in Wiley InterScience (www.interscience.wiley.com).

ABSTRACT: Changes in the molecular orientation, melting behavior, and percent crystallinity of the individual components in a fibrous blend of isotactic polypropylene (iPP) and high-density polyethylene (HDPE) that occur during the melt extrusion process were examined using wide-angle X-ray diffraction (WAXD) and differential scanning calorimetry (DSC). The crystalline orientation of each component was found using Wilchinsky's treatment of uniaxial orientation and described by the Hermans–Stein orientation parameter. The amorphous orientation was found by resolving the X-ray diffraction pattern in steps of the azimuthal angle into its iPP and HDPE crystalline and amorphous reflections. The utility of DSC and WAXD analyses to capture the effects of small differences in processing, and the use of these results as fingerprints of a particular manufacturing process were demonstrated. Major increases in the melting temperatures, percent crystallinities, and molecular orientations of the iPP and HDPE components occurred during the main stretching stage of the melt extrusion process. The annealing stage was found to have little to no effect on the melting behavior and molecular orientation of these components. © 2008 Wiley Periodicals, Inc. J Appl Polym Sci 108: 4047–4057, 2008

Key words: amorphous; orientation; fibers; blends; X-ray

INTRODUCTION

The physical properties and mechanical performance of a polymer fiber are determined by the fiber's molecular characteristics, and the processing conditions have a direct impact on these characteristics. Therefore, it is important to study and understand how the molecular properties are affected by the processing conditions.

Polypropylene and polyethylene fibers are most commonly produced by a melt extrusion process. There are five main steps in this process, which include melting and mixing that occurs in a heated screw-driven chamber, passage through a die, quenching, stretching, and annealing.[1] Each of these steps influences the fiber's final molecular, and therefore mechanical, properties.

Key molecular properties that affect the fiber's mechanical performance are the degree of crystallinity and the molecular orientation. There can be two types of orientation within polymer fibers, including orientation of the crystallites and orientation in the amorphous domain. The amorphous domain refers to the noncrystalline regions of the polymer.[2] It is known that although the orientation in the crystalline phase of semicrystalline polymers plays a major role in determining that fiber's tensile properties, it is not the sole contributor.[3] The orientation in the amorphous phase also plays a significant role in determining these properties.

The main objectives of this study were to determine the molecular orientation, with a focus on the amorphous orientation, of a fibrous blend of isotactic polypropylene (iPP) and high-density polyethylene (HDPE), and to examine the changes in orientation that occur during the melt extrusion process. Amorphous orientation refers to preferential orientation of the molecular segments within the noncrystalline phase. This predominately isotropic phase contains regions of varying degrees of short- to medium-range order. See Figure 1 for a conceptual depiction of amorphous orientation in a polymer fiber.

Polypropylene and polyethylene are immiscible[4,5] and are both semicrystalline. Within the crystalline regions iPP has a monoclinic crystal system with the following unit cell dimensions: a = 0.665 nm, b = 2.096 nm, c = 0.650 nm, and β = 99.3° (b is

**Present address:* New Jersey Center for Biomaterials, Rutgers University, Piscataway, NJ 08854.
Correspondence to: J. W. Zwanziger (jzwanzig@dal.ca).
Contract grant sponsor: AIF.
Contract grant sponsor: NSF; contract grant number: DMR 0513926 (to NSM).

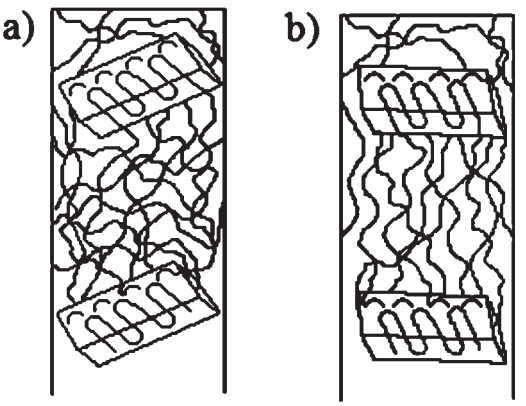

Figure 1 Illustrations of a semicrystalline fiber showing crystallites separated by an amorphous region. (a) No preferential orientation in the amorphous phase. (b) Molecules in the amorphous phase preferentially oriented in the vertical direction.

perpendicular to the *ac* plane).[6] HDPE has an orthorhombic crystal system with $a = 0.7417$ nm, $b = 0.4945$ nm, and $c = 0.2547$ nm.[4] The c axis of the unit cell corresponds to the direction of the molecular chains for both iPP and HDPE.

Differential scanning calorimetry (DSC) was used to investigate the melting behavior and to determine the percent crystallinities of iPP/HDPE fibers at various stages of processing. The crystalline and amorphous orientations were found using wide-angle X-ray diffraction (WAXD). WAXD is routinely used to find the crystalline orientation in semicrystalline polymers,[6–8] but it is rarely used to quantify the amorphous orientation because of the challenges presented by the weak intensity of the amorphous scattering. However, Murthy et al.[2,3] have shown that WAXD can be used to reliably determine the amorphous orientation in semicrystalline polymeric fibers. However, no studies were found in the literature in which WAXD was used to find the amorphous orientation of individual components in a fibrous blend. This study presents a method for finding such orientations in an immiscible semicrystalline blend.

One of the most common techniques used to find the amorphous orientation in polymers is birefringence.[7,9] Birefringence gives information about the overall molecular orientation in a sample, and so to determine the amorphous orientation, the crystallinity and crystalline orientation must be found using other techniques such as DSC and WAXD, respectively. Furthermore, birefringence cannot be used to find the amorphous orientation of individual components within a blend. Even if the crystalline contributions to the birefringence were accounted for, what remained would be the overall amorphous orientation of all amorphous components in the blend. WAXD does not suffer from these shortcomings and can be used as a standalone technique to determine the amorphous orientation of individual immiscible components within a semicrystalline blend.

EXPERIMENTAL

Materials

iPP/HDPE fibers were processed and supplied by two different manufacturers. The fibers were made by a melt extrusion process in which iPP and HDPE resins, with melt flow indexes in the range of 1.2 to 4 g/10 min and 0.6 to 1.1 g/10 min, respectively, were blended together in the melt state. Samples of these fibers were obtained at various points along the melt extrusion lines by both manufacturers. See Figure 2 for a diagram of the extrusion line and the sampling locations. Samples of the fibers were taken immediately after the water quench bath (Stage 0), after the first godet (Stage 1), after exiting the stretching oven (Stage 2), and after exiting the annealing oven (Stage 3). The samples were labeled according to their manufacturer (either A or B) and their stage of extrusion (0, 1, 2, or 3). The processing conditions used at each plant, such as temperatures and draw ratios, were the same.

The fibers are made up of several smaller diameter (~ 1.5 mm) fibers that fused together side-to-side immediately after exiting the die. The width and thickness of the fiber at each sampling location are given in Figure 2. The postproduction fibers are 3000 denier. The major component of the fibers from both manufacturers is iPP, which makes up between 70 and 90% of the blend by mass.

Differential scanning calorimetry

A TA Instruments Q200 DSC was used. Melting endotherms were obtained in a flowing nitrogen atmosphere by heating the samples at a rate of 10°C/min from 70 to 200°C. The sample sizes were between 4 and 6 mg. Aluminum volatile pans were used instead of standard crimped aluminum pans to allow for the shrinkage or expansion of the fibers upon heating. Indium was used as the calibration standard for all of the DSC experiments.

The percent crystallinities were determined by comparing the experimental enthalpy of melting ($\Delta H_{m,\mathrm{exp}}$) of the iPP and HDPE constituents in the blends with the enthalpy of melting for their 100% crystalline forms ($\Delta H_{m,100}$). The ΔH_m for 100% crystalline iPP was cited by Marinelli and Bretas to be 209 J/g.[10] The ΔH_m for 100% crystalline HDPE was

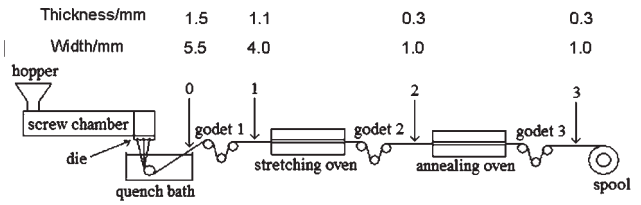

Figure 2 Diagram of the melt extrusion line used to manufacture the iPP/HDPE fibers. The numbers 0 through 3 indicated on the diagram are the points at which samples were obtained. The width and thickness of the fiber at these locations are also given.

reported as 290 J/g.[11] The percent crystallinity for the iPP and HDPE components was found using

$$\% \text{ Crystallinity} = \frac{\Delta H_{m,\text{exp}}}{\Delta H_{m,100}} \times \frac{1}{x} \times 100 \qquad (1)$$

where x is the fraction by mass of the individual component.

X-ray diffraction

2D WAXD patterns were collected using a Bruker AXS's Hi-Star multiwire area detector mounted on a Discover D8 diffractometer and GADDS software. Nickel filtered copper radiation (Cu Kα, $\lambda = 0.1542$ nm) from a Rigaku 18 kW rotating anode with a microfocus filament operated at 50 kV and 50 mA was used. The long-axis of each fiber was positioned perpendicular to the incident X-ray beam. The total data collection time for each fiber was 2 min, although it was found that a rough but workable pattern could be obtained within a few seconds.

The WAXD patterns of the iPP/HDPE blend fibers are merely a superposition of the individual iPP and HDPE patterns because the two parts are immiscible, as previously discussed. This superposition of diffraction patterns was observed by Greco et al.[12] for a PP/PE blend. A consequence of this superposition effect is that the diffractions from iPP and HDPE can be separated and information about the individual constituents can be obtained.

WAXD was used in this study to find both the crystalline and the amorphous orientations of the iPP and HDPE components within the fibers at the various stages of processing. The degree of uniaxial orientation in the crystalline regions was quantified using the Hermans–Stein orientation function,[13]

$$f_c = \frac{3\langle \cos^2 \phi_{c,Z}\rangle - 1}{2}. \qquad (2)$$

f_c is the Hermans–Stein orientation parameter and $\phi_{c,Z}$ is the angle between the c crystallographic axis and the fiber axis. For perfect orientation with the fiber axis, $f_c = 1$. $f_c = 0$ for an isotropic sample or for a sample with average $\phi_{c,Z} = 54.7^\circ$ (the so-called magic angle), and $f_c = -0.5$ for a sample with complete perpendicular orientation with respect to the fiber axis. The angle of 54.7° is known as the magic angle because it is a root of the second-order Legendre polynomial, $P_2(\cos \phi_{c,Z})$, and any parameter proportional to this Legendre polynomial, such as f_c, becomes 0 at this angle.

WAXD was used to find $\langle \cos^2 \phi_{(hkl),Z}\rangle$, the mean squared cosine of the angle between the normal of a particular crystallographic plane and the fiber axis, from the azimuthal intensity distribution, $I(\phi)$, by the following:

$$\langle \cos^2 \phi_{(hkl),Z}\rangle = \frac{\int_0^\pi I(\phi) \sin\phi \cos^2 \phi \, d\phi}{\int_0^\pi I(\phi) \sin \phi \, d\phi}. \qquad (3)$$

$I(\phi)$ was found using a three-parameter Lorentzian squared function

$$I(\phi) = \text{Ampl}\left(\frac{k^2}{(\phi - \text{pos})^2 + k^2}\right)^2, \qquad (4)$$

where k is the half width at quarter maximum, Ampl is the amplitude, and pos is position of the center of the peak. This function was used because it gave a better fit to the data than a Gaussian without having to increase the number of parameters.

Wilchinsky's treatment of uniaxial orientation[14] was simplified according to the symmetry of the unit cells studied and was used to determine $\langle \cos^2 \phi_{c,Z}\rangle$ by WAXD. The simplification of Wilchinsky's treatment for iPP was carried out by Alexander,[6] yielding the following result:

$$\langle \cos^2 \phi_{c,Z}\rangle = 1 - 1.099\langle \cos^2 \phi_{(110),Z}\rangle - 0.901\langle \cos^2 \phi_{(040),Z}\rangle. \qquad (5)$$

A similar simplification was carried out for HDPE using two intense HDPE ($hk0$) reflections that were present in the fiber WAXD patterns. These were the (110), at $2\theta = 21.6^\circ$, and the (200), at $2\theta = 24.0^\circ$, reflections. Because of the orthorhombic symmetry of HDPE's unit cell and the type of reflections studied, Wilchinsky's treatment was simplified to

$$\langle \cos^2 \phi_{c,Z}\rangle = 1 - 0.5555\langle \cos^2 \phi_{(200),Z}\rangle - 1.445\langle \cos^2 \phi_{(110),Z}\rangle. \qquad (6)$$

To describe the molecular orientation in the amorphous phase, the Hermans–Stein orientation function [eq. (2)] can be rewritten as

$$f_{\mathrm{am}} = \frac{3\langle \cos^2 \phi \rangle - 1}{2}, \quad (7)$$

where f_{am} is the amorphous orientation parameter. f_{am} describes the degree to which the anisotropic portion of the amorphous phase is oriented. The quantitative interpretation of f_{am} is analogous to that of f_c.

f_{am} gives information about the anisotropic portion of the amorphous phase, but another parameter is needed to describe how much of the amorphous phase is anisotropic. Murthy et al.[2] proposed the following function to find the fraction of the oriented amorphous phase, F_{oa}, using the azimuthal intensity distribution of the amorphous scattering,

$$F_{\mathrm{oa}} = \frac{A_p}{A_p + A_b} \quad (8)$$

where A_p is the area under the peak and A_b is the area under the baseline. F_{oa} is not a measure of the amorphous content of the material but is a measure of the total fraction of the amorphous phase that is preferentially oriented. Both F_{oa} and f_{am} were used in this study to characterize the amorphous phase.

f_{am} was quantified by fitting the anisotropic portion of the azimuthal intensity distribution with a Lorentzian squared function [eq. (4)]. The resultant fit was plugged into eq. (3) with $\langle \cos^2 \phi \rangle$ in place of $\langle \cos^2 \phi_{(hkl),Z} \rangle$. Finally, the value of $\langle \cos^2 \phi \rangle$ was used to solve eq. (7). Finding the azimuthal intensity distribution of the amorphous scattering is not as straightforward as the process for the crystalline reflections, because the amorphous scattering is buried under the crystalline peaks. Therefore, before the amorphous peak could be fitted, it had to be isolated from the other peaks. The process used for obtaining the amorphous azimuthal intensity distribution is discussed in more detail in the ''X-ray diffraction: Amorphous orientation'' (Results) section.

The apparent crystallite sizes of iPP and HDPE were calculated from the WAXD patterns using the Scherrer equation[15]:

$$D_{hkl} = \frac{0.9\lambda}{\beta \cos\theta}, \quad (9)$$

where D_{hkl} is the apparent crystallite size in the (hkl) direction, λ is the wavelength of the incident X-ray beam, β is the full width at half-maximum (FWHM) in 2θ in units of radians, and θ is the diffraction angle. A constant of 0.9 was used as is commonly done when β is the FWHM. The crystallite size calculated from a meridonal reflection using the Scherrer equation, because the reflection is broadened by lattice defects, strain, and distortions, provides a lower limit of the lamellar thickness.

RESULTS AND DISCUSSION

Differential scanning calorimetry

DSC was used to find the melting points and the percent crystallinities of the iPP and HDPE components of the fiber samples from both manufacturers (A and B). The melting endotherms of the fibers from A and B are shown in Figure 3(a,b), respectively. All of the melting endotherms contained two main peaks. The first peak, which displays a melting point around 135°C, is due to the HDPE in the fiber and the second peak, with a melting point of ~ 165°C, is due to the iPP in the fiber.

The presence of two separate melting peaks observed for the iPP/HDPE fibers confirmed that the crystalline regions of iPP and HDPE were immiscible and that these polymers did not cocrystallize. Because of this fact, the melting point and percent crystallinity for both components were able to be determined (see results in Table I). If they were miscible and did cocrystallize then only one melting peak would be present. The immiscibility of PP/HDPE blends is well known and has been well studied for the crystalline regions[4,5,16–18] and has also

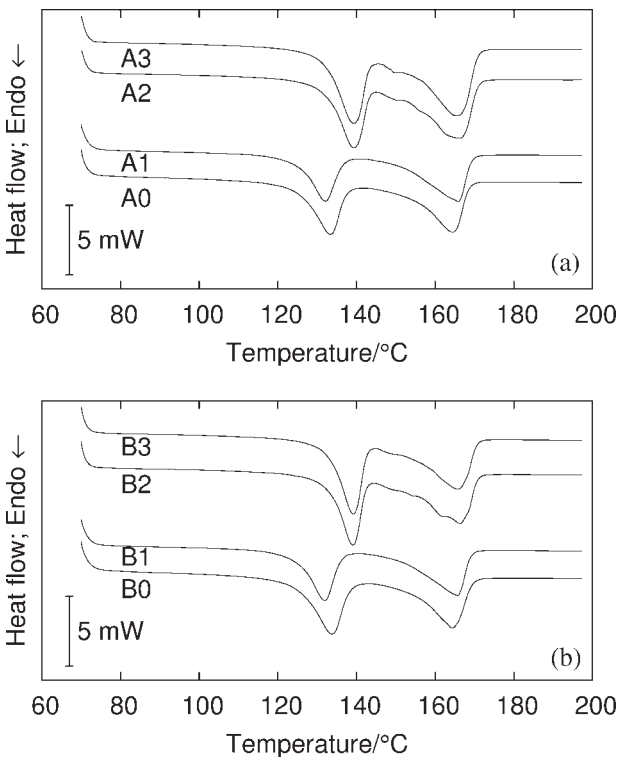

Figure 3 Melting endotherms for iPP/HDPE fibers at various stages of processing from (a) Company A (A) and (b) Company B (B).

TABLE I
Melting Points (T_m) and Percent Crystallinites for iPP/HDPE Fibers from Company A (A) and Company B (B) at Various Stages of Processing

	Sample		Stage 0	Stage 1	Stage 2	Stage 3
T_m (°C)	A	iPP	165	165	167	166
		HDPE	133	132	139	139
	B	iPP	165	166	166	166
		HDPE	134	132	139	139
Crystallinity (%)	A	iPP	35	35	45	44
		HDPE	67	57	73	74
	B	iPP	31	34	46	45
		HDPE	64	56	73	79

been found in the amorphous regions and the melt state.[5,17,18]

Because of the broad temperature range over which the iPP and HDPE components melt, the melting temperature, T_m, was treated as the temperature at which the maxima in the endothermic melting peak occurred. This is a common treatment for the melting point of polymers analyzed by DSC.[19]

These results show that the melting behaviors of the fibers from the two different manufacturers, who used similar processing conditions, were nearly identical. The major change in the iPP and HDPE components of the fibers occurred during the main stretching stage. In both the A and B fibers the melting point of HDPE increased significantly from about 133°C before stretching to about 139°C after stretching. The increase in melting point was accompanied by an increase of $\sim$ 16% in percent crystallinity. In this stage the fibers were heated to a temperature below that at which HDPE begins to melt as they were stretched to a high elongation. In effect, this stage is a combined annealing and stretching stage. The heating and stretching increases the molecular motion and leads to molecular rearrangement. This allows a significant portion of the molecules in the amorphous phase to rearrange into their more thermodynamically stable crystalline forms, which accounts for the observed increase in percent crystallinities.

Increased molecular motion can also have the effect of reducing the crystalline defects, which form because of the rapid cooling of the melt during the quenching stage, and increasing the thicknesses of the lamellae. Thicker lamellae with a higher degree of perfection melt at a higher temperature than thin lamellae with many defects.[20]

During the final annealing stage of processing, the fibers were heated to a slightly higher temperature than before but still below the onset of melting of HDPE. This was done to remove any additional defects and to further increase the percent crystallinity of the fibers. However, it was found that the melting points did not change significantly and that only the percent crystallinity of the HDPE in the B fiber increased and that of the A fiber remained the same, while the percent crystallinities of iPP actually decreased slightly. The lack of change in the melting points suggest that the majority of the crystalline defects were removed in the previous stage and that there was no further increase in the thickness of the thickest lamellae. The precise cause for the difference in percent crystallinities between manufacturers is unclear.

The reason why the changes in melting points and percent crystallinities of the iPP component of the fibers were not as drastic as those observed for the HDPE component may be that the heating temperature was much less than the melting point of iPP and was closer to the melting point of HDPE. This would have resulted in less molecular motion of iPP, but when combined with stretching it was still significant for some of the amorphous phase to rearrange into crystallites as evidenced by the more than 10% increase in percent crystallinity between Stages 1 and 2. HDPE also crystallizes more readily than iPP because it lacks any stericly hindering side-chain groups and can therefore pack together more easily. This is why in every fiber the percent crystallinity of HDPE is greater than that of iPP.

The melting behavior of the iPP component was much more complex than the melting behavior of the HDPE as seen in Figure 3(a,b). The occurrence of a multiple-melting endotherm for iPP is common and has been extensively studied, yet there is still some question as to its exact origin.[20–24] There are thought to be two main causes for this behavior, including the melting of lamellae with different thicknesses and degrees of perfection,[20–22] and the presence of different crystalline forms such as α (monoclinic), β (hexagonal), and γ (triclinic).[23,24] The β and γ forms are metastable with respect to the α form. The latter of the two possibilities was ruled out by WAXD as only reflections from the α form were observed (see later).

The rapid quenching of the fibers in the water bath during the melt extrusion process most likely produced imperfect crystal lamellae with different thicknesses. This is seen in the broad melting peaks of iPP in A0, A1, B0, and B1. After heating and stretching, the occurrence of multiple-melting peaks became more pronounced (especially in the B2 fiber) because of the effects of increased molecular motion during these processes, as previously discussed.

Two minor lower temperature iPP melting peaks appeared in the melting endotherm of A2 and B2. This was probably due to the creation of thinner lamellae as some of the amorphous phase rearranged to form crystallites. Upon annealing, the minor peak at $\sim$ 155°C disappeared and was not

TABLE II
Lateral Crystallite Sizes (D_{110}) of iPP and HDPE in iPP/HDPE Fibers from Company A (A) and Company B (B) at Various Stages of Processing

Sample		D_{hkl} in the (110) direction (nm)			
		Stage 0	Stage 1	Stage 2	Stage 3
A	iPP	11	11	9.1	7.9
	HDPE	18	16	14	14
B	iPP	10	10	8.3	8.0
	HDPE	19	20	14	16

Errors: ±10%.

present in the melting endotherms of A3 or B3. This may have been the result of the thickening of these lamellae and subsequent melting at a higher temperature. To confirm these suspected causes a more detailed study employing the use of microscopy would need to be conducted.

Using eq. (9) the crystallite sizes of iPP and HDPE in the fibers at each of the stages of processing were determined from the WAXD patterns. No meridonal reflections were present in the WAXD patterns so the lamellar thickness of iPP and HPDE could not be determined, but strong (110) equatorial reflections were present for both iPP and HPDE. Using these reflections the lateral crystallite sizes were found (see results in Table II). The decrease in apparent crystallite size for both iPP and HDPE is due to residual strain generated during drawing. These results cannot be directly correlated to changes observed in the fiber melting endotherms because of the effect of residual strain on the WAXD patterns and the fact that the melting points are influenced more strongly by the lamellar thickness than the lateral crystallite size.

X-ray diffraction: iPP crystalline orientation

The Bragg reflections appeared as diffuse rings in the WAXD patterns of the fiber samples that had not gone through the main stretching stage of processing [see Fig. 4(a)]. For the fiber samples that did go through the main stretching stage, the intense Bragg reflections appeared as narrow peaks [see Fig. 4(b)]. This change indicates that the degree of orientation dramatically increased as the fiber was stretched.

The (110) and (040) reflections were azimuthally scanned using the program Datasqueeze[25] from 0° to 360°, where 0° was set as the position of the fiber axis. The scans were plotted as intensity versus azimuthal angle and were fitted with a linear baseline and Lorentzian squared functions. A linear baseline was required to account for the underlying amorphous scattering and the Lorentzian squared functions were used to describe the crystalline reflections.

Because of the cylindrical symmetry of the diffraction pattern, only one fitted peak was analyzed. See Figure 5(a,b) for the fitted scans of A3 (110) and A0 (040), respectively. The integrals of eq. (3) were evaluated numerically from 0° to 180° for stretched samples and from 90° to 180° for the others. The diffraction pattern from 0° to 90° is equivalent to the pattern from 90° to 180° due to symmetry. The stretched samples were evaluated from 0° to 180° even though this was not necessary because it was easier to analyze the entire peak as opposed to half of it. The less-oriented samples could not be analyzed from 0° to 180° because of the location of the beam stop.

The iPP crystalline orientations found from these scans are recorded in Table III. The values of the crystalline orientation for iPP were very similar between the two manufacturers at the same stage of processing. From these results it can be seen that as the fiber exited the quench bath, the iPP component had a minor degree of preferential orientation toward the direction perpendicular to the fiber axis. At the exit of the first set of godets, the iPP crystallites became more oriented in the fiber axis direction, but at this stage there was still only a minor degree of

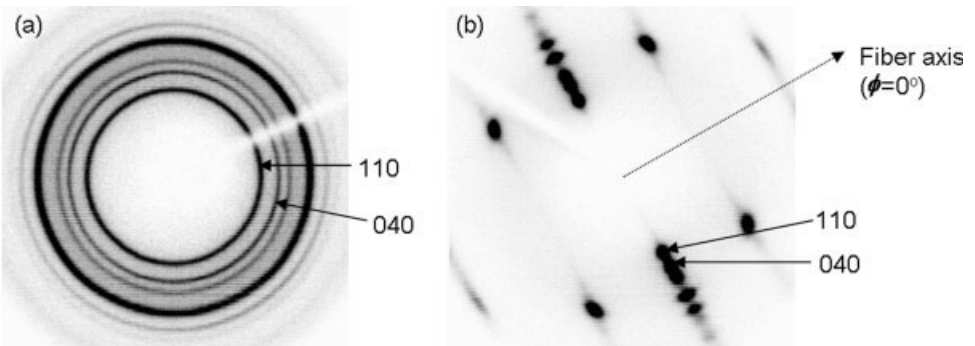

Figure 4 (a) WAXD pattern of A0. The first intense ring out from the center of the image is the iPP (110) reflection, and the second is the iPP (040) reflection. (b) WAXD pattern of A3. The first intense spot out from the center of the image is the iPP (110) reflection, and the second is the iPP (040) reflection.

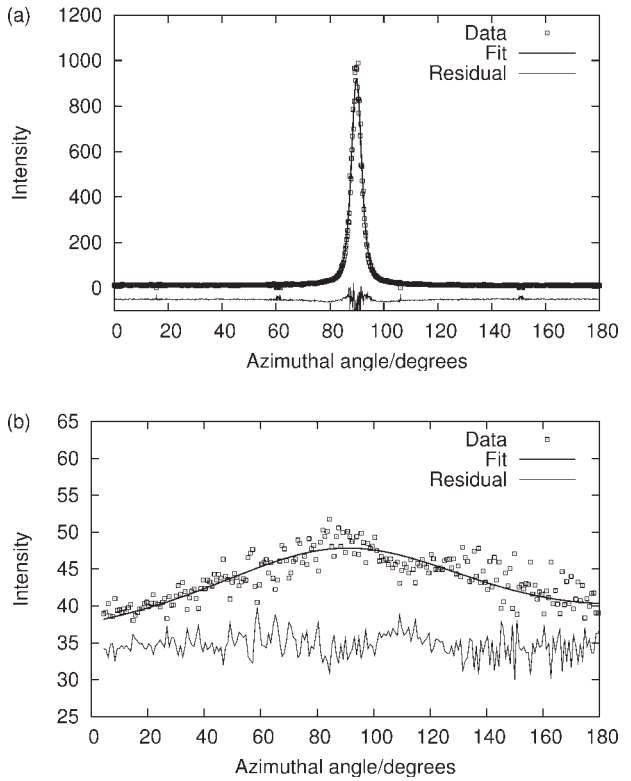

Figure 5 Azimuthal scans and fits of intense iPP Bragg reflections. (a) (110) reflection of the A3 sample and (b) (040) reflection of the A0 sample. The residual was offset from zero for clarity.

orientation. At the exit of the stretching oven, the greatest change in orientation of iPP was observed. At this stage the crystallites were nearly perfectly aligned with the fiber axis. There was no change observed between the orientation directly before and after exiting the annealing oven. The HDPE reflections were masked by the iPP reflections, and so a simple azimuthal scan could not be used to determine the crystalline orientation for this component.

X-ray diffraction: Amorphous orientation

To determine the amorphous orientation of iPP and HDPE their azimuthal intensity distributions were found. Ideally it is necessary to obtain the azimuthal intensity distribution with the sample positioned at the proper $\theta/2\theta$ orientation for each reflection studied. However, the data obtained with the fiber and the detector perpendicular to the incident beam provide valid results for comparing the orientations of two fibers that are not very different from each other, as is true with the A and B samples. To obtain the amorphous azimuthal intensity distributions for a particular sample the WAXD pattern was radially scanned using the program Datasqueeze in steps of the azimuthal angle, ϕ. For these scans the position of the equatorial axis was set as $\phi = 0^\circ$. Half of the WAXD patterns of the unstretched samples (samples from Stages 0 and 1) were radially scanned in steps of 5°, starting at the position of the fiber axis, giving a total of 37 radial scans per sample. See Figure 6 for a diagram showing the position of the fiber axis, the equatorial axis, and a representative radial scan for the WAXD pattern of A3.

Starting at the position of the fiber axis, the diffraction patterns of the stretched samples (from Stages 2 and 3) were scanned in steps of 10°, then in steps of 5°, and in steps of 2° nearest to the equatorial axis with one scan centered on the equatorial axis. This was done for half of the entire diffraction pattern giving a total of 32 scans per sample. More scans were taken around the equatorial axis to ensure that there would be enough points to fully describe the equatorial reflections.

For each sample, every scan was resolved into its crystalline and amorphous peaks. The number and initial position of the peaks were assigned according

TABLE III
Crystalline Orientation, Described by the Hermans–Stein Orientation Parameter (f_c), of the iPP Component of the iPP/HDPE Blend Fibers

Sample		f_c
A0	iPP	−0.0402
A1	iPP	0.157
A2	iPP	0.991
A3	iPP	0.991
B0	iPP	−0.112
B1	iPP	0.147
B2	iPP	0.990
B3	iPP	0.990

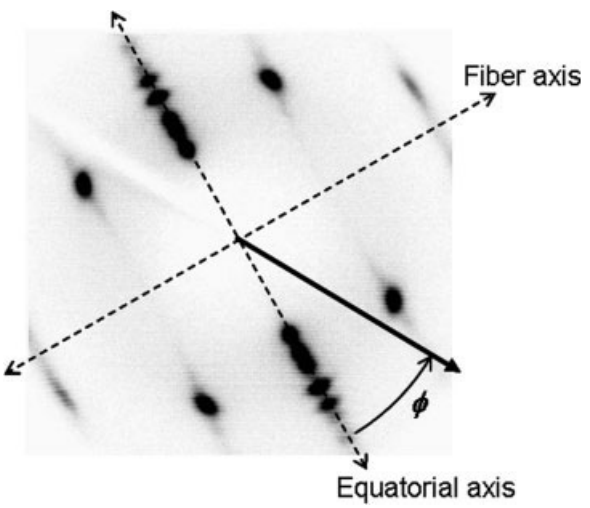

Figure 6 WAXD pattern of a stretched fiber showing the position of the fiber axis and the equatorial axis. ϕ is the azimuthal angle. Radial scans of the pattern were performed at regular intervals of ϕ with a fixed value of ϕ for each scan. The solid arrow depicts one such radial scan. The scan was performed along the arrow's length.

to those found in the literature.[26–28] The full diffraction pattern of each sample contained 11 crystalline Bragg reflections and two amorphous reflections. Because of the diffuse ring-like Bragg reflections, each scan of the unstretched samples contained all of the reflections and was modeled using 13 peaks, including one iPP and one HDPE amorphous peak. The Bragg reflections of the stretched samples were much narrower, and consequently, the scans did not contain all of the reflections. The scans were, therefore, modeled using two amorphous peaks and between zero and seven crystalline peaks depending on the azimuthal angle of the scan. A Lorentzian squared function was used for each peak.

Nonlinear least squares minimization was used to fit the peaks to the diffraction pattern of each scan. The position and width of the peaks were allowed to vary within narrow constraints, while the amplitude was allowed to vary unconstrained. See Figure 7(a,b) for the resultant full resolution of the $\phi = -80^\circ$ scans of B1 and B2, respectively. The broad peaks centered at $\sim 16^\circ$ and 20.5° are correspondingly due to the amorphous scattering of iPP and HDPE. The crystalline peaks were allowed to vary by approximately plus or minus 0.2° away from their initial positions, while the amorphous peaks were allowed to vary by approximately plus or minus 1.5°. This was done because the positions of amorphous peaks are known to shift considerably with changes in the azimuthal angle.[2,3]

The amplitudes of the amorphous peaks from a fitted scan were used as the measure of the intensities of the peaks at that particular ϕ. Each scan resulted in one point of intensity versus azimuthal angle for the amorphous iPP and HDPE scattering. The results of all of the scans were combined to get the full azimuthal intensity distributions.

The azimuthal intensity distributions were fitted with a linear baseline, which represented the isotropic amorphous regions, and a Lorentzian squared function, which described the anisotropic portion of the amorphous phase. See Figure 8 for the fitted amorphous azimuthal intensity distributions of B1 and B2.

The azimuthal intensity distributions of both components were used to solve for their amorphous orientation parameters, as previously discussed in the ''X-ray diffraction'' (Experimental) section, and to solve for their fractions of oriented amorphous phase using eq. (8). A prominent feature in the amorphous azimuthal intensity distributions of even the most highly stretched fibers is the nonzero baseline indicative of the isotropic portion of the amorphous phase. The results are shown in Table IV and Figure 9.

The fibers from the first two stages of processing were found to have no regions of preferential orientation within the amorphous phase, indicating that the amorphous phase of these unstretched fibers is purely isotropic. There was a large change in both f_{am} and F_{oa} after the fibers went through the main stretching stage. The heating that occurred during this stage allowed for increased molecular motion and the uniaxial stretching forced molecules in portions of the amorphous phase to align in the draw direction. It was found that there is a fairly small but significant fraction of oriented amorphous phase in the stretched fibers and that this fraction has a high degree of preferential orientation with respect to the fiber axis.

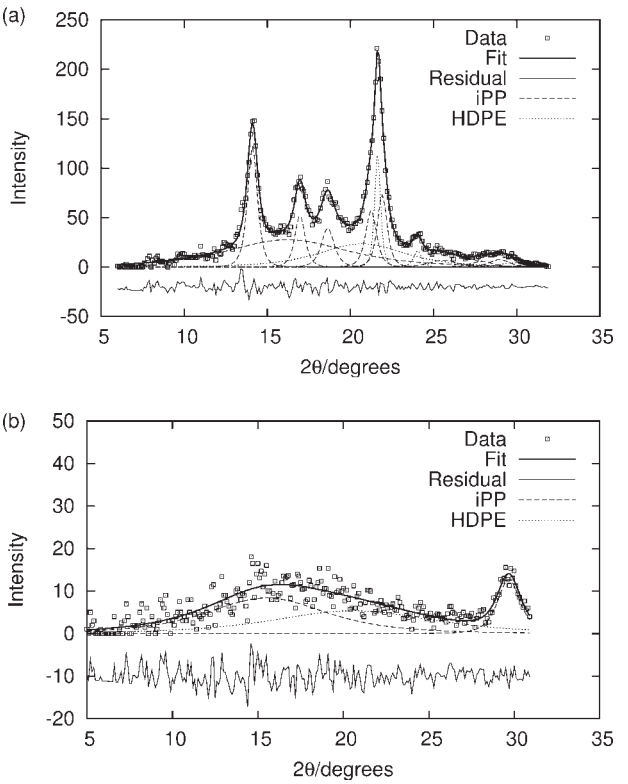

Figure 7 (a) The full resolution of the $\phi = -80^\circ$ radial scan of B1 using two amorphous and 11 crystalline peaks. (b) The full resolution of the $\phi = -80^\circ$ radial scan of B2 using one crystalline and two amorphous peaks. The residual was offset from zero for clarity.

Between Stages 2 and 3 there was very little to no change in the degree of amorphous orientation of either the iPP or HDPE components. This was to be expected because there was no additional stretching of the fibers during the annealing process. This is consistent with the similar lack of change between these two stages that was found for the crystalline orientation of iPP. All of the fibers showed a small decrease in F_{oa} upon annealing. The decrease was greater for iPP than it was for HDPE. Therefore, annealing did not enhance the desirable molecular properties of the amorphous phase.

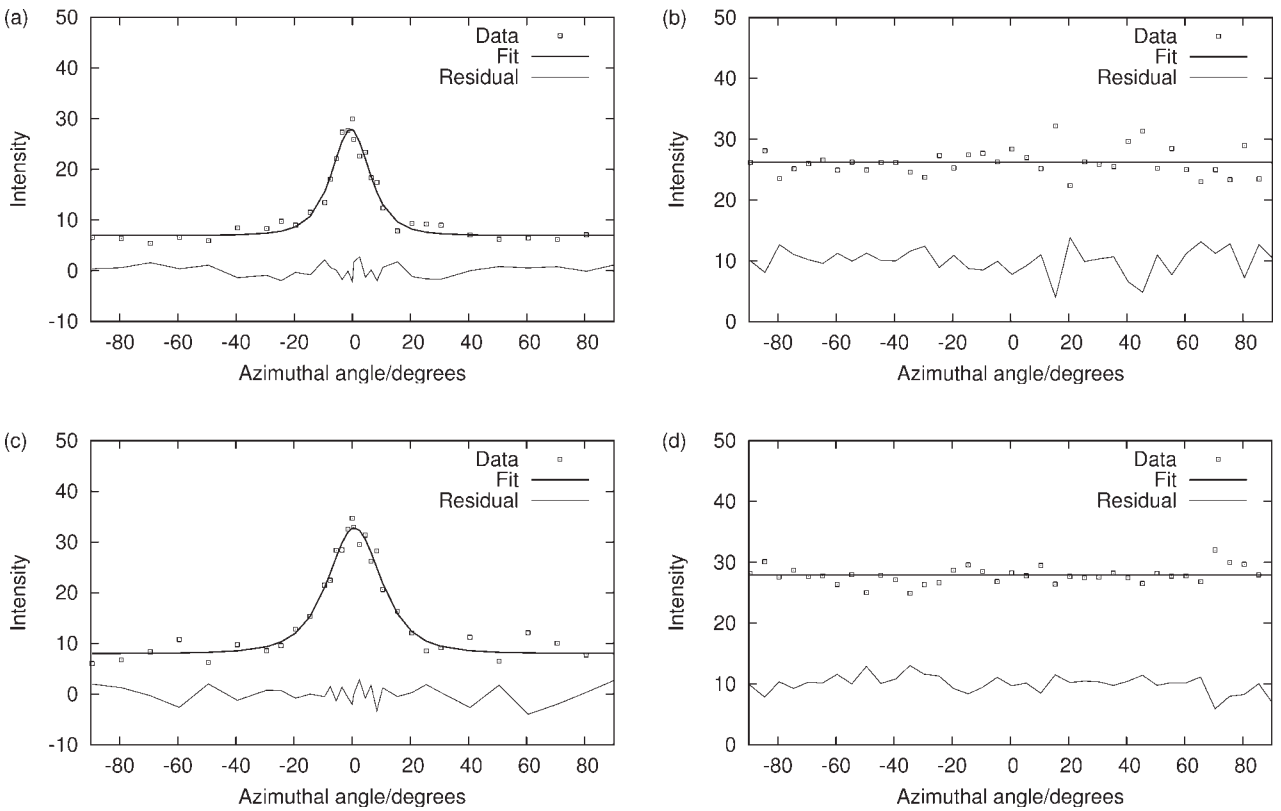

Figure 8 Fitted amorphous azimuthal intensity distributions of (a) the HDPE component of B2 (a highly stretched fiber), (b) the HDPE component of B1 (an unstretched fiber), (c) the iPP component of B2, and (d) the iPP component of B1. The residual was offset from zero for clarity.

f_{am} was greater for the HDPE than the iPP component in each of the stretched samples. Because of the absence of side-chain groups, the molecules of HDPE can efficiently pack together. The side-chain methyl groups of iPP could make it more difficult for the molecular chains to align as uniaxially as those of HDPE, and consequently, result in a lower f_{am} value.

It was also found that the HDPE in the stretched B fibers had a larger fraction of oriented amorphous phase but that this fraction had a lower degree of orientation than the HDPE in the A fibers. There were no significant differences in the amorphous orientations of the iPP component between the two manufacturers.

TABLE IV
Amorphous Orientation, Described by the Amorphous Orientation Parameter (f_{am}), and the Fraction of Oriented Amorphous Phase (F_{oa}) of the iPP and HDPE Components of the iPP/HDPE Blend Fibers

	Sample		Stage 0	Stage 1	Stage 2	Stage 3
f_{am}	A	iPP	0	0	0.88	0.87
		HDPE	0	0	0.97	0.97
	B	iPP	0	0	0.87	0.89
		HDPE	0	0	0.92	0.92
F_{oa}	A	iPP	0	0	0.28	0.24
		HDPE	0	0	0.13	0.12
	B	iPP	0	0	0.31	0.27
		HDPE	0	0	0.24	0.22

X-ray diffraction: HDPE crystalline orientation

$\langle \cos^2 \phi_{(200),Z} \rangle$ was found by performing a simple azimuthal scan of the diffraction pattern similar to those done for the iPP reflections. However, this

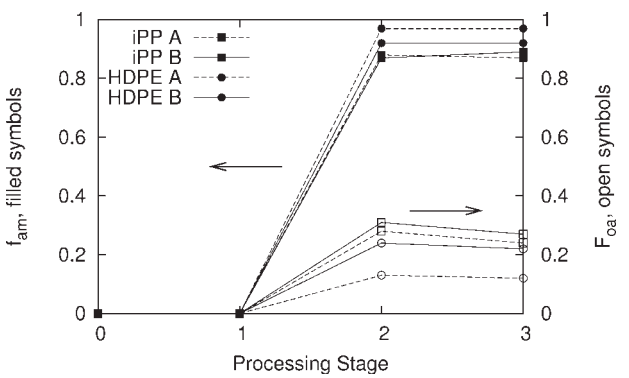

Figure 9 Changes in the amorphous orientation parameter (f_{am}) and the fraction of oriented amorphous phase (F_{oa}) with processing. Dashed and solid lines are used to indicate the results for Company A and Company B fibers, respectively.

could not be done for the (110) reflection because it was masked by two iPP reflections with similar values of 2θ. The azimuthal intensity distribution of the (110) reflection was, therefore, found using the same radial scans and the same procedure as that used for the amorphous scattering with $\phi = 0^\circ$ set as the position of the fiber axis. See Figure 10(a) for the fitted (110) azimuthal intensity distribution of B2 and Figure 10(b) for the fitted (110) azimuthal intensity distribution of B1.

The azimuthal intensity distributions of the (110) HDPE crystalline reflections have a baseline of zero and can be fully described by either one [as in Fig. 10(a)] or two [as in Fig. 10(b)] Lorentzian squared functions. The results of the crystalline orientation of the HDPE component in the fibers are shown in Table V.

The results show that the values of crystalline orientation of HDPE were similar for the two manufacturers at the same stage of processing. This was also seen for the crystalline orientation values of iPP. Only a small degree of orientation was found for the unstretched fibers, and once again, the major change occurred after the fibers went through the main stretching stage of processing. The crystalline regions of HDPE in the stretched fibers were found to be almost perfectly aligned with the fiber axis, and like the degree of crystalline orientation of iPP and the amorphous orientation of both iPP and HDPE, there was no change brought about by annealing.

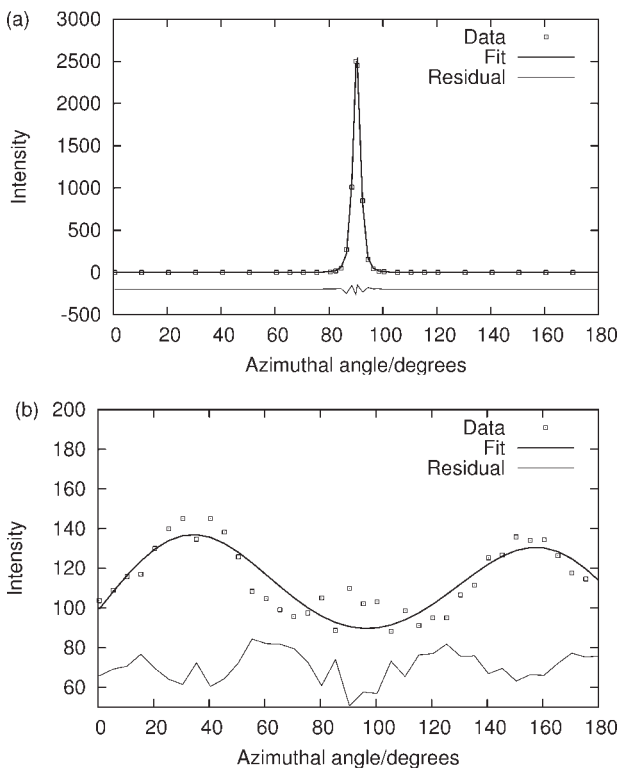

Figure 10 Fitted HDPE (110) azimuthal intensity distributions of (a) B2 and (b) B1. The residual was offset from zero for clarity.

TABLE V
Crystalline Orientation, Described by the Hermans–Stein Orientation Parameter (f_c), of the HDPE Component of the iPP/HDPE Blend Fibers

Sample		f_c
A0	HDPE	0.0999
A1	HDPE	0.133
A2	HDPE	0.995
A3	HDPE	0.995
B0	HDPE	0.0499
B1	HDPE	0.0717
B2	HDPE	0.995
B3	HDPE	0.995

The values obtained for both the crystalline and amorphous orientations of the stretched fibers are higher than those normally achieved for iPP and HDPE by melt spinning. Previous investigators have obtained maximum values for the crystalline orientation factor of ~ 0.6[29] to 0.9[30] and 0.7[29,31] for melt spun iPP and HDPE fibers, respectively. More recently, Gregor-Svetec obtained a maximum value for melt spun polypropylene fibers of ~ 0.9 for the crystalline orientation factor and 0.8 for the amorphous orientation factor.[8]

The nearly perfect molecular orientation in the crystalline and anisotropic amorphous regions of the fibers we investigated was a result of the highly specialized melt extrusion process used by the manufacturers. It should be made aware that although the amorphous orientation parameter is near unity, this only describes the orientation of the anisotropic amorphous region, and there is still a significant portion of these fibers, that is, the isotropic amorphous portion that exhibited no preferential orientation.

CONCLUSIONS

Using the discussed experimental procedure WAXD can be used as a nondestructive offline, but potentially online, method for detecting subtle differences in fibers due to processing. This method can be used to not only detect subtle differences in fibers at various stages of processing but also to examine the underlying differences in fibers produced by different manufacturers. It could be used to isolate the cause for variations in the final mechanical properties of fibers from different extrusion batches and manufacturers and would aid in eliminating the need for tedious trial and error methods of optimizing extrusion line processing conditions. The time required for data acquisition and analysis is on the order of tens of minutes and hours, respectively. From these data all orientation information can be obtained.

In this study, WAXD was successfully used to determine the amorphous and crystalline orientations of the individual components within a semicrystalline fibrous blend of iPP and HDPE at various stages of processing from two manufacturers. The major changes in the molecular orientation and melting behavior of both components of the fibers occurred during the main stretching stage of the melt extrusion process. After the main stretching stage, the crystallites of these components were nearly perfectly aligned with the fiber axis.

At the early stages of processing the amorphous phase was completely isotropic, but after being heated and stretched a small portion of the amorphous phase was highly oriented with respect to the fiber axis. There was little to no change in the crystalline and amorphous orientations of iPP and HDPE after the fibers were annealed and there was a slight drop in the fraction of oriented amorphous phase. The melting points and percent crystallinities of iPP and HDPE increased during the main stretching stage, but only the percent crystallinity of HDPE in the B fiber increased upon annealing.

The authors thank M. A. White and her group at Dalhousie University for allowing use of their differential scanning calorimeter, and P. A. Heiney for technical support. A. Trottier thanks NSERC for an undergraduate student research award.

References

1. Giles, H. F.; Wagner, J. R.; Mount, E. M. Extrusion—The Definitive Processing Guide and Handbook; William Andrew Publishing: Norwich, NY, 2005; Chapter 51.
2. Murthy, N. S.; Bray, R. G.; Correale, S. T.; Moore, R. A. F. Polymer 1995, 36, 3863.
3. Murthy, N. S.; Bednarczyk, C.; Rim, P. B.; Nelson, C. J. J Appl Polym Sci 1997, 64, 1363.
4. Teh, J. W.; Rubin, A.; Keung, J. C. Adv Polym Tech 1994, 13, 1.
5. Choi, P.; Blom, H. P.; Kavassalis, T. A.; Rudin, A. Macromolecules 1995, 28, 8247.
6. Alexander, L. E. X-Ray Diffraction Methods in Polymer Science; Wiley: New York, 1969; Chapter 4.
7. Penning, J. P.; van Ruiten, J.; Brouwer, R; Gabriëlse, W. Polymer 2003, 44, 5869.
8. Gregor-Svetec, D. J Appl Polym Sci 2006, 100, 1067.
9. Despar, C. R.; Southern, J. H.; Ulrich, S. D.; Porter, R. S. J Appl Phys 1970, 41, 4284.
10. Marinelli, A. L.; Bretas, R. E. S. J Appl Polym Sci 2003, 87, 916.
11. Wunderlich, B. Macromolecular Physics, Vol. 3; Academic Press: New York, 1980; p 58.
12. Greco, R.; Mucciariello, G.; Ragosta, G.; Martuscelli, E. J Mater Sci 1980, 15, 845.
13. Stein, R. S. J Polym Sci 1958, 31, 327.
14. Wilchinsky, Z. W. Advances in X-Ray Analysis, Vol. 6; Plenum Press: New York, 1963; p 231.
15. Klug, H. P.; Alexander, L. E. X-Ray Diffraction Procedures; Wiley: New York, 1954; Chapter 9.
16. Jose, S.; Aprem, A. S.; Francis, B.; Chandy, M. C.; Werner, P.; Alstaedt, V.; Thomas, S. Eur Polym J 2004, 40, 2105.
17. Li, J.; Shanks, R. A.; Olley, R. H.; Greenway, G. R. Polymer 2001, 42, 7685.
18. Shanks, R. A.; Li, J.; Yu, L. In Imaging and Image Analysis Applications for Plastics; Pourdeyhimy, P., Ed.; Plastics Design Library: Norwich, NY, 1999, p 59.
19. Simon, G. P. Polymer Characterization Techniques and Their Application to Blends; Oxford University Press: New York, 2003; Chapter 2.
20. Zhu, X.; Yan, D.; Tan, S.; Wang, T.; Yan, D.; Zhou, E. J Appl Polym Sci 2000, 77, 163.
21. Kim, Y. C.; Ahn, W.; Kim, C. Y. Polym Eng Sci 1997, 37, 1003.
22. Zhang, F.; Gong, Y.; He, T. Eur Polym J 2003, 39, 2315.
23. Paukszta, D.; Garbarczyk, J. Fibres Text East Eur 2003, 11, 50.
24. Al-Raheil, I. A.; Qudah, A. M.; Al-Share, M. J Appl Polym Sci 1998, 67, 1267.
25. Heiney, P. A. CPD Newslett 2005, 32, 9.
26. Murthy, N. S. Polym News 1991, 16, 358.
27. Murthy, N. S.; Minor, H. Polymer 1990, 31, 996.
28. Karacan, I. J Appl Polym Sci 2006, 101, 1317.
29. Spruiell, J. E.; White, J. L. Polym Eng Sci 1975, 15, 660.
30. Nadella, H. P.; Henson, H. M.; Spruiell, J. E.; White, J. L. J Appl Polym Sci 1977, 21, 3003.
31. Dees, J. R.; Spruiell, J. E. J Appl Polym Sci 1974, 18, 1053.